

Thermal dehydration kinetics and characterization of synthesized potassium borates

Miguel Ortega Asensio¹ · Meral Yildirim² ·
Fatma Tugce Senberber² · Azmi Seyhun Kipcak² ·
Emek Moroydor Derun²

Received: 3 August 2015 / Accepted: 17 October 2015 / Published online: 29 October 2015
© Springer Science+Business Media Dordrecht 2015

Abstract In this study, potassium pentaborate (santite: $\text{KB}_5\text{O}_8 \cdot 4\text{H}_2\text{O}$), with a powder diffraction number of 01-072-1688 was synthesized from potassium carbonate (K_2CO_3), boric acid (H_3BO_3) and boron oxide (B_2O_3) with reaction efficiencies between 84.88 and 95.11 %, through a hydrothermal route. Reaction temperatures and times were varied between 60–90 °C and 15–120 min. Synthesized minerals were characterized by X-ray diffraction, Fourier transform infrared and Raman spectroscopies, while surface morphologies were determined by scanning electron microscopy. Thermal dehydration behavior of santite was determined by thermal gravimetry and differential thermal analysis. From the results, santite lost its crystal water via a two-step process between 50 and 450 °C. Activation energies (E_a) were calculated by using four non-isothermal kinetic methods and found to be 110.12 and 202.43 kJ/mol by the Coats–Redfern method, 107.77 and 304.18 kJ/mol by the Doyle method, 158.82 and 154.50 kJ/mol by the Kissinger–Akahira–Sunose method, and 158.07 and 156.76 kJ/mol by the Ozawa–Flynn–Wall method for the steps 1 and 2, respectively.

Keywords Hydrothermal · Non-isothermal kinetic · Potassium borate · Thermal dehydration

✉ Emek Moroydor Derun
moroydor@gmail.com; moroydor@yildiz.edu.tr

¹ Department of Chemical Engineering, Universidad de Valladolid, Valladolid, Spain

² Department of Chemical Engineering, Faculty of Chemical and Metallurgical Engineering, Yildiz Technical University, Davutpasa Campus, Davutpasa Street No. 127, Esenler, 34210 Istanbul, Turkey

Introduction

Boron never appears as a free element in nature, but it can form very different compounds by comparatively small changes in the solution's mineral content. Turkey hosts about 72.2 % (870 million tons) of the worldwide known reserves of boron. Among these reserved metal borates has been one of the groups of borate minerals subjected to continuous research, making up a wide diversity of industrial usage areas, including glass, ceramics, nuclear, space-aviation, metallurgy, transportation, cosmetics and chemistry [1, 2].

Different sub-classes can be commonly grouped, such as calcium borates, calcium–sodium borates, sodium borates and magnesium borates [3]. However, many synthetic borate compounds have been studied and used in industry apart from the ones that can be found in nature. Potassium pentaborate ($\text{KB}_5\text{O}_8 \cdot 4\text{H}_2\text{O}$) is widely used as one of the important borates, as it contains 4 mol of structural water per mole of crystal. It is called tetrahydrate potassium pentaborate, commonly known as santite. It has acquired importance among fields such as metal refining, welding, lubricating oil additives, cement, insulation, textiles, fiberglass and as a superior non-linear optical material (NLO) against commonly used borate compounds [4–6].

Among the literature [7–16], it is possible to find several studies on the synthesis of potassium pentaborate. However, most of these methods [8–11] focus on the solid-state field, using high temperatures (800–1400 °C) and long reaction times to produce potassium borate crystals. MacDonald et al. [8] reacted potassium carbonate (K_2CO_3) and boron oxide (B_2O_3) at 1400 °C, while Hasim et al. [11] and Alajeram et al. [9] used a reaction temperature of 1200 °C for the reaction of boric acid (H_3BO_3) and K_2CO_3 . In the experiments conducted by Binu et al. [10], a mixture of K_2CO_3 and B_2O_3 was melted at 830 °C. Despite its efficiency, solid-state synthesis has corrosion and handling problems due to the melting of the potassium borates [12]. The hydrothermal type of synthesis has raised interest among these production methods, as back in 1935 Gale [7] was one of the first who attempted to create an industrial method for high efficiency preparation by reacting potassium chloride (KCl) and $\text{Na}_2\text{B}_{10}\text{O}_{16}$ in a 35 °C hydrothermal mixture for the synthesis of $\text{K}_2\text{B}_{10}\text{O}_{16}$. More recent studies such as those by Belokoneva et al. [13] and Wang et al. [14] were performed at higher temperatures and pressures with Belokoneva using 280 °C, 70 atm and Wang using 165 °C. Rajasekar et al. [15] produced $\text{KB}_5\text{O}_8 \cdot 4\text{H}_2\text{O}$ by dissolving K_2CO_3 and B_2O_3 and Gurbuz et al. [16] used a 1:5 (as $\text{B}_2\text{O}_3/\text{K}_2\text{O}$) molar ratio mixture to produce anhydrous potassium pentaborate. Therefore, it has been found that most of the available literature focuses on really high temperatures and long reaction times.

Dehydration is the process of removing water from a hydrate structure at a certain temperature. It can be used for different technological and economical purposes, in research for thermal properties, decreasing the mass of hydrate minerals during transport, or it can be a necessary stage of a chemical process [17]. Dehydration reactions are strongly endothermic and many are reversible. In some dehydration examples, the process may occur in several steps, including water

elimination and structural recrystallization of the residual product (lower hydrate or anhydrous salt) [18]. Thermal dehydration behaviors of hydrate borate minerals have been studied widely due to the notable properties of boron minerals. There are some studies of thermal kinetics for the different types of hydrated borates such as H_3BO_3 [19], ulexite ($\text{NaCaB}_5\text{H}_{16}\text{O}_{17}$) [17], sodium borate hydrate ($\text{NaB}(\text{OH})_4 \cdot 2\text{H}_2\text{O}$) [20], mcallisterite ($\text{Mg}_2(\text{B}_6\text{O}_7(\text{OH})_6)_2 \cdot 9(\text{H}_2\text{O})$) [21], admontite ($\text{MgO} \cdot 3\text{B}_2\text{O}_3 \cdot 7\text{H}_2\text{O}$) [22], inderite ($\text{MgB}_3\text{O}_3(\text{OH})_5 \cdot 5\text{H}_2\text{O}$) [23], zinc borate hydrate ($\text{Zn}_3\text{B}_6\text{O}_{12} \cdot 3.5\text{H}_2\text{O}$) [24], lithium borate [25], howlite ($\text{Ca}_2\text{B}_5\text{SiH}_5\text{O}_{14}$) [26] and tunellite ($\text{SrB}_6\text{H}_8\text{O}_{14}$) [26, 27].

As can be seen in the literature for the hydrothermal route, potassium borates can be synthesized at very high reaction temperatures and times so the first novelty of this paper is to synthesize a pure $\text{KB}_5\text{O}_8 \cdot 4\text{H}_2\text{O}$ (santite) mineral with very low reaction temperatures and reaction times by comparison with the literature using the hydrothermal method. The reactor type and crystallization temperature used in the experiments were the same as in the studies of both Derun and Senberber [21] and Derun et al. [22]. Synthesis parameters were selected to focus on the wide ranges of 60–90 °C and 15–120 min, together with the achievement of high reaction yields from the samples. Following the synthesis, the characterization of the minerals have been done by X-ray diffraction (XRD), Fourier transform infrared (FT-IR) and Raman spectroscopies, while surface morphologies were determined by scanning electron microscopy (SEM). The second novelty of this paper is the determination of the thermal dehydration behavior, such as: reaction order, activation energy and exponential factor for dehydration steps of santite, which have not previously been reported in the literature. Thermal dehydration behavior is determined by the equipment of thermal gravimetry and differential thermal analysis (TG/DTA).

Materials and methods

Raw material preparation

In synthesis, H_3BO_3 and B_2O_3 were used as boron sources, and were obtained from Bandırma Boron Works (Eti Maden, Balıkesir, Turkey) and sieved through a Fritsch analysette 3 Spartan pulverisette 0 vibratory sieve-shaker (Fritsch, Idar-Oberstein, Germany) (particle size < 75 μm) after being subjected to crushing and grinding by a Retsch RM 100 (Retsch, Haan, Germany). The potassium source was K_2CO_3 which was supplied by Sigma-Aldrich, St. Louis, USA (CAS Number 584-08-7, with a minimum purity of 99 %) and used without any pretreatment. Identification studies of raw materials were carried out by a Philips PANalytical XPert Pro (PANalytical, Almelo, The Netherlands) X-ray diffractometer (XRD) at 45 kV and 40 mA ($\lambda = 1.53 \text{ cm}^{-1}$) by using Cu-K α radiation in the 2θ range of 7°–90°.

Hydrothermal synthesis

Two different sets were conducted to synthesize potassium borates, using different sources of boron minerals. For set 1, the used boron source was H_3BO_3 , while B_2O_3

was used for set 2. In both sets, K_2CO_3 was used as the potassium source. The reaction temperature and time ranges selected were 60–90 °C and 15–120 min, respectively.

The nucleation cell used during the experiments was a 105-ml glass reactor, covered with the proper lid. The nucleation cell was kept on a thermal platform and the temperature was controlled using a thermocouple with an accuracy of 0.1 °C. In order to achieve a homogeneous temperature and a proper concentration in the entire reactor, a magnetic stirrer located in the thermal platform was used.

In the set 1 and set 2 experiments, the optimum raw material ratio of elemental potassium to elemental boron was determined as 1:5 and 1:6, respectively. The resulting crystal formations were found to be quite different depending both on the molar ratio and on the different temperatures and reaction times used. Generally, low molar ratios and low temperatures lead to a more amorphous crystal and a less homogeneous pattern [28]. For set 1 in the optimum molar ratio, 12.94×10^{-3} mol of H_3BO_3 was dissolved in 50 mL of deionized water obtained from a GFL 2004 (Gesellschaft für Labortechnik, Burgwedel, Germany) water purification system in a reactor at a determined reaction temperature. Then, 1.29×10^{-3} mol of K_2CO_3 was added. In set 2, in order to maintain the same stoichiometric amount of boron in set 1, 6.46×10^{-3} mol of B_2O_3 was used along with 1.08×10^{-3} mol K_2CO_3 . After the required reaction time, the mixture was removed from the nucleation cell and placed in a crystallizer glass and allowed to evaporate in a controlled atmosphere of 40 °C for 48 h, which is enough time for crystallization to occur.

The resulting crystals were removed from the crystallizer, ground, and then purified by ethanol to remove the excess of H_3BO_3 . The samples were allowed to dry at 40 °C in an incubator (EcoCell LSIS-B2V/EC55; MMM Medcenter Einrichtungen, Planegg, Germany) and then weighed and analyzed. Expected

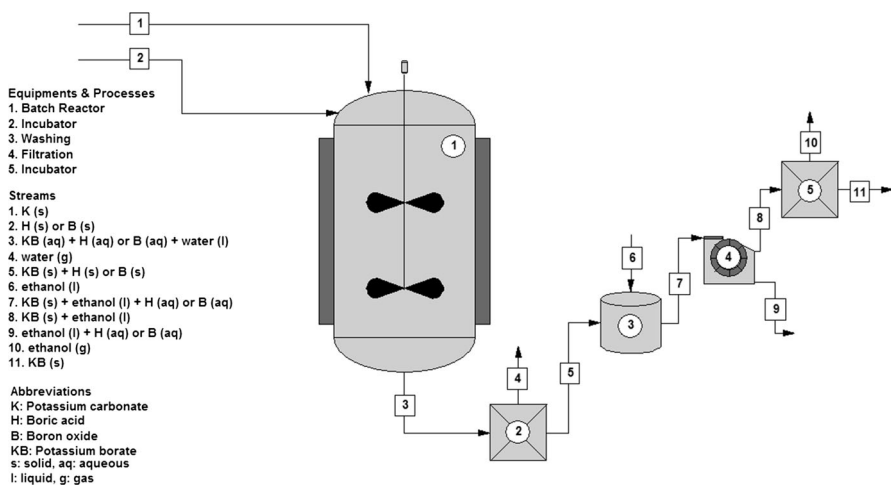
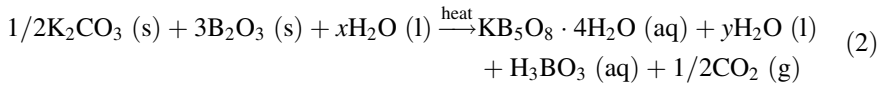
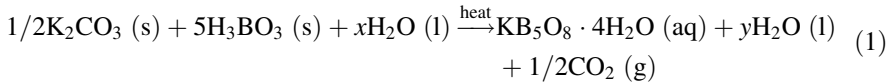


Fig. 1 Reaction scheme

reaction equations are shown in Eqs. (1) and (2). The reaction scheme is shown in Fig. 1.



Characterization

After the synthesis processes, the synthesized compounds were identified by XRD, FT-IR and Raman spectroscopy techniques. The XRD parameters used as same as in “Raw material preparation” except 2θ range was selected between 10° – 90° . The characteristic peaks of the borate compounds were in the range 1500 – 500 cm^{-1} [28, 29]. Based on the literature, for FT-IR and Raman spectroscopies, the spectrum ranges were determined as 1800 – 650 and 1800 – 250 cm^{-1} , respectively. FT-IR analyses were carried out by a PerkinElmer Spectrum One FT-IR (PerkinElmer, MA, USA) with a universal attenuation total reflectance (ATR) sampling accessory with a diamond/ZnSe crystal. A Perkin Elmer brand Raman Station 400F (PerkinElmer) was used for Raman spectroscopy, which, coupled with vibrational (FT-IR) spectroscopy, enabled observations on the molecular structure of the potassium borate mineral.

The surface morphologies and particle properties of the synthesized compounds were investigated by using a CamScan Apollo 300 field-emission SEM (CamScan, Oxford, UK) at 20 kV. The detector used was back scattering electron (BEI) and the magnification was set to 10,000.

Reaction yields

The reaction yields were calculated using the method given by Derun et al. [22] and Kipcak et al. [1, 30–32]. In this method, K_2CO_3 were identified as the key component in the first and second sets of experiments.

Specifically, the number of moles of product at the final stage, N_D , was divided by the number of consumed moles of the key reactant, A , to calculate the overall yield, Y_D (3). The number of moles of A that were consumed was calculated using the initial (N_{A0}) and final (N_A) moles of the reactant. For a batch system, the equation becomes [33]

$$Y_D = \frac{N_D}{N_{A0} - N_A} \quad (3)$$

The calculations of the reaction yields were completed in triplicate.

Thermal dehydration kinetics

The thermal dehydration behavior of potassium borate mineral was studied between temperatures of 50 and 550 °C with a PerkinElmer Diamond TG/DTA (PerkinElmer). The thermal behavior of the synthesized potassium borate mineral was subjected to different heating rates (β) of 5, 15, and 20 °C/min in an inert (N₂) atmosphere. Kinetic parameters such as the activation energy (E_a) and exponential factor (k_0) were calculated by Coats–Redfern, Doyle, Kissinger–Akahira–Sunose (KAS) and Ozawa–Flynn–Wall (OFW) non-isothermal kinetic methods.

In the Coats–Redfern kinetic method, data from the TG curve in the dehydration range were used to determine the kinetic parameters. These were calculated using the plot of conversion (α) as a function of temperature (T). The Coats–Redfern kinetic method equations are given by (4) and (5):

$$\ln\left(-\frac{\ln(1-\alpha)}{T^2}\right) = \ln\left(\frac{k_0R}{\beta E_a}\right) - \frac{E}{RT} \quad n = 1 \quad (4)$$

$$\ln\left(-\frac{1-(1-\alpha)^{1-n}}{(1-n)T^2}\right) = \ln\left(\frac{k_0R}{\beta E_a}\right) - \frac{E}{RT} \quad n \neq 1 \quad (5)$$

In the Doyle kinetic method, kinetic parameters were calculated by using the peak temperatures of the DTA curves. The values of $-\log \beta$ were plotted against $1/T_m$. The slope of line was $0.4567 \times E/R$. The equation for the Doyle kinetic method is given by (6) and (7):

$$-\log \beta = 0.4567 \times \frac{E_a}{RT_m} + \text{constant} \quad (6)$$

$$k_0 = \frac{\beta E_a}{RT_m^2} \times e^{\frac{E_a}{RT_m}} \quad (7)$$

The KAS kinetic model uses the same approximation as the Coats–Redfern method and determines kinetic parameters from the plots which are drawn $\ln(\beta/T^2)$ versus $1/T$ where k_0 is the exponential factor, $g(\alpha)$ is the integral conversion kinetic function, R is gas constant and E_a is activation energy (8).

$$\ln \frac{\beta}{T^2} = \ln \frac{k_0 E_a}{g(\alpha) R} - \frac{E_a}{RT} \quad (8)$$

The OFW kinetic model (9) gives the kinetic parameters from a plot of the logarithm of heating rates versus $1/T$ for a given value of conversion at various heating rates (β).

$$\ln \beta = \ln \frac{0.0048 k_0 E_a}{g(\alpha) R} - 1.0516 \frac{E_a}{RT} \quad (9)$$

The highest scored potassium borate was calcined in a Protherm MOS 180/4 high-temperature furnace under a nitrogen atmosphere flowing at 5 mL/min in order to investigate the thermal conversion of the potassium borate mineral. Prior to thermal analysis, calcination temperatures were determined as 450 and 550 °C. Crystal lattice structures of calcined minerals were identified by XRD and changes in morphologies were studied by SEM.

Results and discussion

Results of the raw material characterization

According to the XRD results of raw materials, the potassium source was identified as the mixture of three different crystal structures of “potassium carbonate (K_2CO_3)” with the powder diffraction file numbers (pdf nos.) of: 00-049-1093, 00-016-0820 and 01-087-0730. The XRD results of the boron sources showed that H_3BO_3 was defined as sassolite (H_3BO_3) with pdf no. of 01-073-2158 and B_2O_3 was determined to be a mixture of two types of boron oxide with the pdf nos. of 00-006-0297 and 01-088-2485.

XRD results of the synthesized potassium borates

The synthesized potassium borate XRD results are given in Table 1, from which it can be seen that, at all reaction temperatures and reaction times, santite ($KB_5O_8 \cdot 4H_2O$) mineral, which is a special kind of potassium borate, was

Table 1 XRD scores of potassium borates synthesized from K_2CO_3 , H_3BO_3 and B_2O_3

Temperature (°C)	Time (min)	Set 1 (K-H)	Set 2 (K-B)
60	15	74	60
60	30	67	62
60	60	54	60
60	120	63	51
70	15	54	60
70	30	65	63
70	60	51	59
70	120	59	62
80	15	61	59
80	30	64	62
80	60	62	62
80	120	62	62
90	15	58	65
90	30	58	54
90	60	47	52
90	120	57	60

synthesized. Its pdf no. is 01-072-1688 and crystallized in the orthorhombic crystal structure. The detailed crystallographic data for santite are given in Table 2.

Synthesized products were coded as; “set code—reaction temperature—reaction time” and “K–H” for the set of “ $K_2CO_3:H_3BO_3$ ” and “K–B” for the set of “ $K_2CO_3:B_2O_3$ ”. For example, the product synthesized with the conditions of 90 °C reaction temperature and 15 min of reaction time using $K_2CO_3:H_3BO_3$ was coded as “K-H-90-15”. The highest XRD score—when all the peak intensities (%) and peak locations are matched perfectly with the reference card, the XRD score of the analyzed mineral is equal to 100—are obtained at the reaction temperature of 60 °C and 15 min of reaction time in set 1 with a value of 74. On the other hand, in set 2, the highest XRD score was found to be 65 at 90 °C reaction temperature and 15 min of reaction time. From the results, generally higher XRD scores were obtained at lower reaction temperatures and reaction times. Also, it can be seen that higher XRD scores were obtained in set 1 than in set 2. Optimum products (with higher XRD scores) were obtained in the parameters of K-H-90-15, K-H-80-30, K-H-70-30 and K-H-60-15 in set 1 and K-B-90-15, K-B-80-30, K-B-70-30 and K-B-60-30 in set 2. These optimum XRD patterns of the products are given in Fig. 2, from which the characteristic peaks [h k l ($d_{spacing}$)] of santite can be observed at the 2θ positions of 14.92° [1 1 1 (5.93 Å)], 15.85° [0 2 0 (5.59 Å)], 25.32° [0 2 2 (3.51 Å)], 26.59° [1 2 2 (3.35 Å)], 32.35° [4 0 0 (2.77 Å)] and 41.52° [4 2 2 (2.17 Å)].

FT-IR and Raman spectral analysis results of the synthesized products

FT-IR spectra of optimum potassium borate compounds are shown in Fig. 3. For all parameters, FT-IR spectra of synthesized potassium borates are similar.

For IR peaks between 1332 and 1328 cm^{-1} are ascribed to asymmetric stretching of three coordinate boron to oxygen bands [$\nu_{as}(B_{(3)}-O)$], whereas the bending mode of boron–oxygen–hydrogen [$\delta(B-O-H)$] are fitted in the range of 1247 – 1245 cm^{-1} . The peaks between 1095 and 1021 cm^{-1} are assigned to asymmetric stretching of

Table 2 Crystallographic data of santite

Mineral name	Santite
Reference code	01-072-1688
Chemical formula	$KB_5O_8 \cdot 4H_2O$
Molecular weight (g/mol)	293.20
Crystal system	Orthorhombic
Space group	Aba2 (No. 41)
a (Å)	11.0620
b (Å)	11.1750
c (Å)	9.0410
α (°)	90.00
β (°)	90.00
γ (°)	90.00
z	4.00
Density (calculated, g/cm^3)	1.74

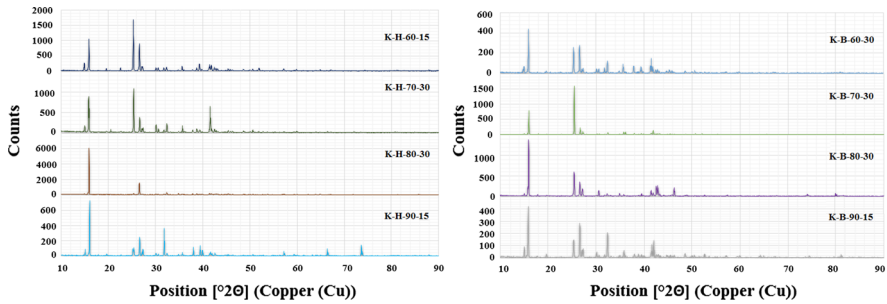


Fig. 2 XRD patterns of the synthesized optimum potassium borates

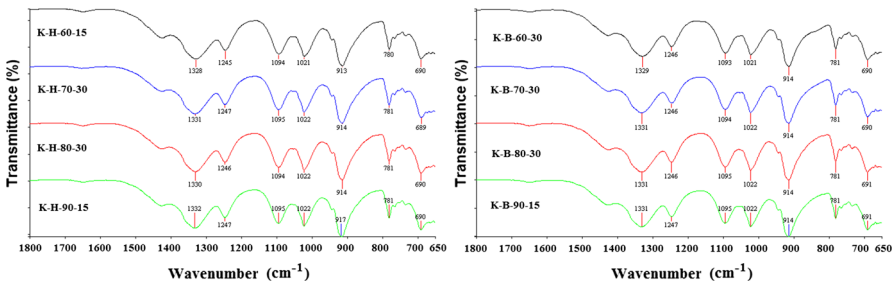


Fig. 3 FT-IR spectra of optimum potassium borates

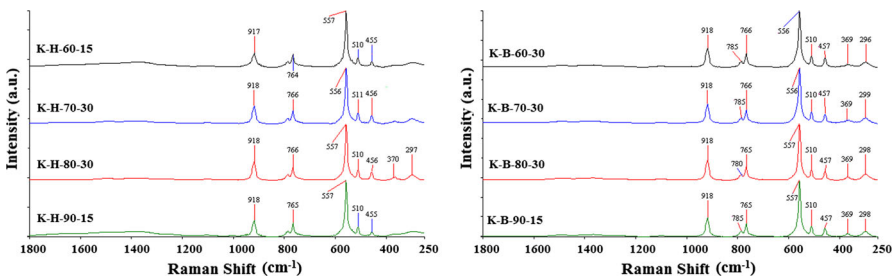


Fig. 4 Raman spectra of selected potassium borates

four coordinate boron to oxygen bands [$\nu_{as}(\text{B}_{(4)}\text{-O})$]. The symmetric stretching of three coordinate boron to oxygen bands [$\nu_s(\text{B}_{(3)}\text{-O})$] is observed at around 913 cm^{-1} . The frequency at 780 cm^{-1} belongs to symmetric stretching of four coordinate boron to oxygen bands [$\nu_s(\text{B}_{(4)}\text{-O})$]. Bending of three-coordinate boron [$\delta(\text{B}_{(3)}\text{-O})$] is observed at 690 cm^{-1} . Figure 4 shows the Raman spectra of optimum potassium borates. According to the Raman spectra, around 918 cm^{-1} the vibrations are caused by $\nu_s(\text{B}_{(3)}\text{-O})$, when the frequencies between 766 and 764 cm^{-1} are symmetric stretching of $\nu_s(\text{B}_{(4)}\text{-O})$. The peak around 557 cm^{-1} is assigned to the symmetric pulse vibration frequency of the pentaborate anion [$(\text{B}_5\text{O}_6(\text{OH})_4)^-$]. The

Raman frequencies between 510 and 297 cm^{-1} belong to bending of four-coordinate boron $\delta(\text{B}_{(4)}\text{-O})$. The obtained FT-IR and Raman bands were in accordance with the results obtained by Jun et al. [29].

SEM morphologies

SEM surface morphologies of optimum potassium borates are given in Fig. 5a, b for set 1 and set 2, respectively. According to the SEM images, the particle sizes of the synthesized potassium borates were changed between 667.67 nm and 5.98 μm . For the K–H set, the particle size increases with increasing reaction time; also, at the low temperatures, the particle size distribution is seen to be more uniform than the higher temperatures. At both 60 and 70 $^{\circ}\text{C}$, the product particles have multiangular and overlapped shapes. In the second set of K–B, when the reaction temperature was set to 60 $^{\circ}\text{C}$, a layered and dust-like particle texture is the obtained while for the other reaction temperature the potassium borate particles have irregular particle morphologies and less sharp edges.

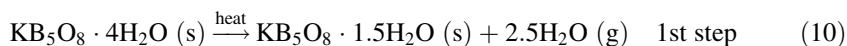
Reaction yield results

Figure 6 shows the reaction yields of the synthesized potassium borates. In both sets, the reaction yields increased with increasing temperature and reaction times. In the sets, higher reaction yields were observed at 90 $^{\circ}\text{C}$ and lower reaction yields at 60 $^{\circ}\text{C}$. Reaction yields were calculated to be between 93.49 and 95.11 and 84.88 and 89.27 %, for the sets of K–H and K–B, respectively. Highest reaction yields were found to be 95.11 ± 0.5 and 89.27 ± 0.6 % for the sets of K–H and K–B, respectively.

Thermal dehydration behavior

Thermal analysis results for dehydration behavior of $\text{KB}_5\text{O}_8 \cdot 4\text{H}_2\text{O}$ are given in Table 3 and Figs. 7 and 8. The mineral lost its crystal water via a two-step process between the temperatures of 50 and 450 $^{\circ}\text{C}$. The first two endothermic peaks seen in the DTA curves were in compatible with the peaks in the DTG curves. Although the dehydration process ended at approximately 450 $^{\circ}\text{C}$, there was a third peak in the DTA curves in the range of 450–550 $^{\circ}\text{C}$ which indicates the recrystallization of the dehydrated structure.

The probable reactions for the dehydration process are given in Eqs. (10) and (11). According to the thermal analyses results (Table 3), the first step of dehydration had the approximate initial temperature of 105 $^{\circ}\text{C}$ while the final temperature varied in the range of 175.16–207.11 $^{\circ}\text{C}$. The average weight loss was 15.22 % for the first step, equal to a value of 2.5 mol of water.



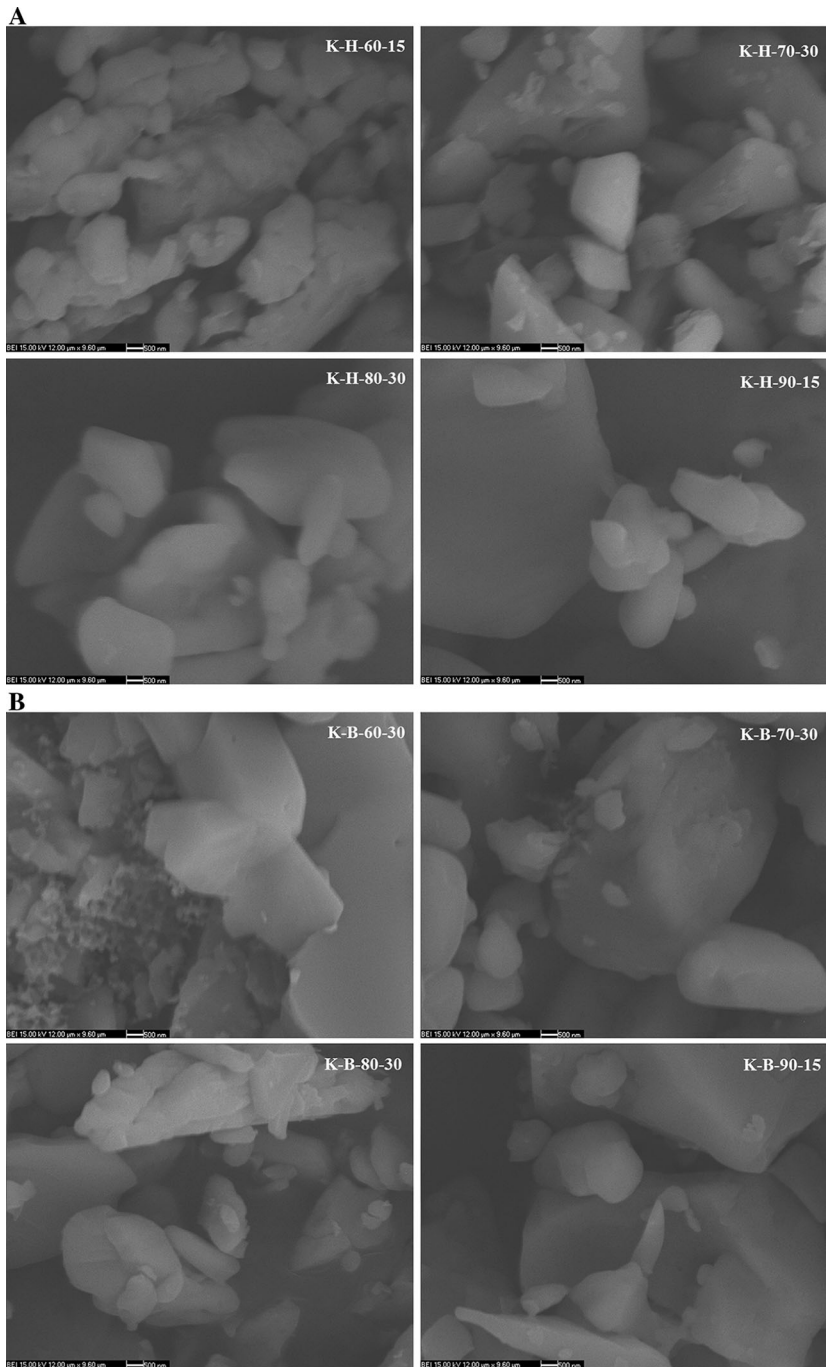


Fig. 5 **a** SEM morphologies of the optimum potassium borates obtained from K–H. **b** SEM morphologies of the optimum potassium borates obtained from K–B

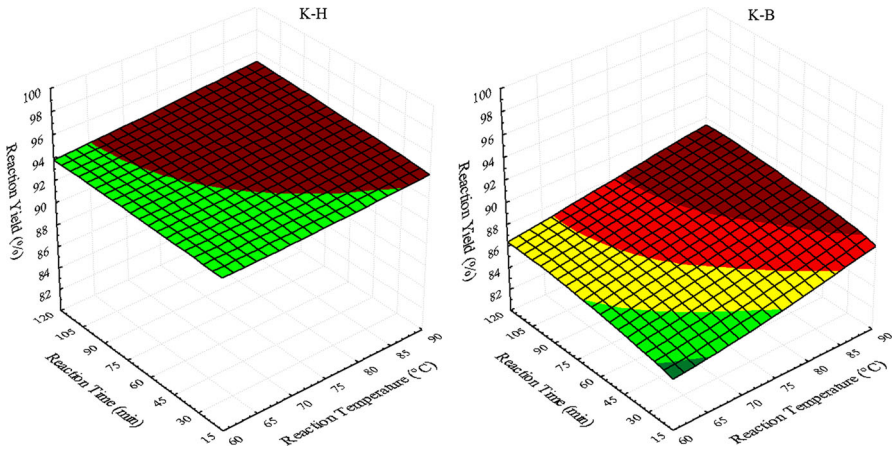
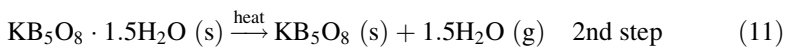


Fig. 6 Reaction yields of potassium borates

Table 3 Thermal analyses result of K-H-60-15

Heating rate (°C/min)		5	15	20
TG				
1st step	T_{Initial} (°C)	105.07	105.41	105.71
	T_{Final} (°C)	175.16	201.26	207.11
	Mass loss (%)	14.98	15.96	15.34
2nd step	T_{Initial} (°C)	175.16	201.26	207.11
	T_{Final} (°C)	449.71	450.00	450.84
	Mass loss (%)	8.87	8.35	9.05
	Total mass loss (%)	23.85	24.31	24.39
DTG				
1st step	T_{Initial} (°C)	101.19	102.36	105
	T_{peak} (°C)	151.72	165.74	168.85
	T_{Final} (°C)	175.14	184.68	185.05
2nd step	T_{Initial} (°C)	175.14	184.68	185.05
	T_{peak} (°C)	194.62	197.04	210.22
	T_{Final} (°C)	218.08	239.88	251.92
DTA				
1st step	T_{peak} (°C)	152.00	166.01	171.60
2nd step	T_{peak} (°C)	201.86	208.21	210.21
3rd step	T_{peak} (°C)	492.67	504.02	504.64



The second step started at the final temperature of the first step and ended at a temperature around 450 °C. The average weight loss was 8.98 % for the second

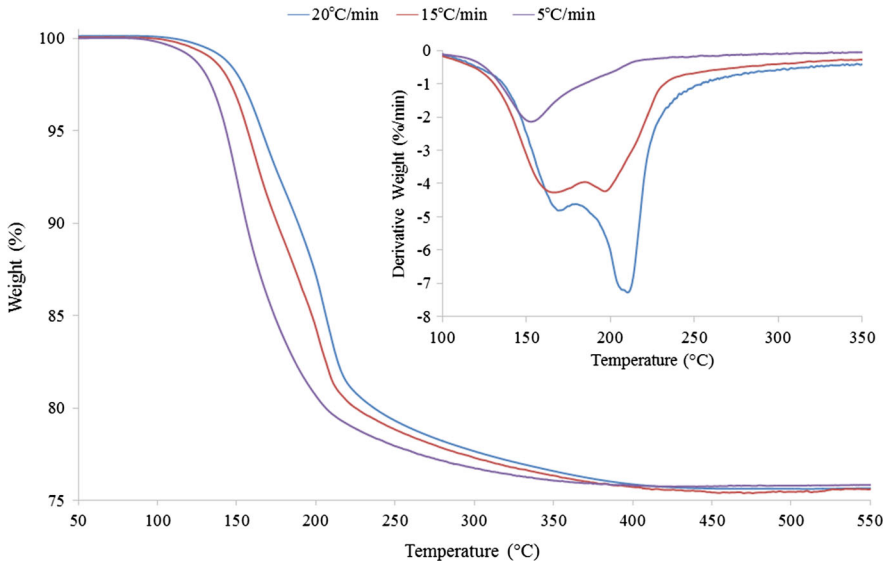


Fig. 7 TG and DTG curves of K-H-60-15

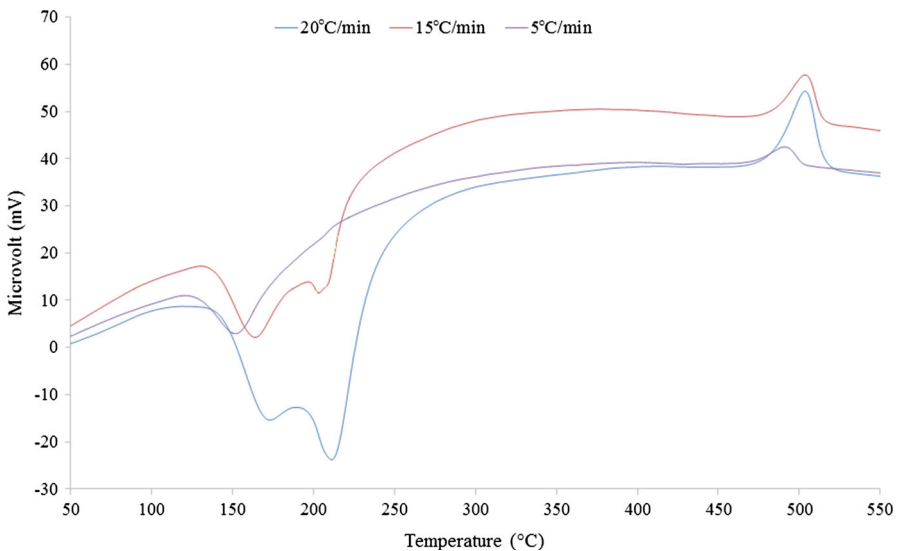
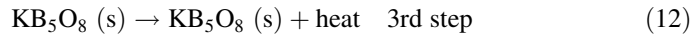


Fig. 8 DTA curve of K-H-60-15

step, equal to a value of 1.5 mol of water. The total average weight loss was 24.19 %.

From the thermal conversion results, calcined santite at 450 and 550 °C lost approximately 24.50 % of its initial weight. This result was in mutual agreement

with the TG analyses, which is equal to 4 molar equivalents of structural water content. The loss in the structural water content indicates that the santite lost all of its structural water at 450 °C and transformed into a dehydrated type of potassium borate-type compound with a pdf no. of 01-070-1402. After that temperature, its lattice parameters were changed and it transformed to another type of dehydrated potassium borate mineral with a pdf no. of 01-076-1367 at 550 °C, which has the same formula. The probable equation at the recrystallization step (around 500 °C) is given in Eq. (12).



The crystallographic data and XRD patterns for the calcined products are shown in Table 4 and Fig. 9, respectively.

From Fig. 9, the characteristic peaks [h k l (d_{spacing})] of 550 °C calcined (01-076-1367) potassium borate were observed at the 2θ positions of 20.24° [1 2 1 (4.38 Å)], 23.97° [2 0 0 (3.71 Å)], 24.16° [0 0 4 (3.68 Å)], 25.16° [2 1 0 (3.53 Å)], 26.50° [1 3 1 (3.36 Å)], 31.15° [2 1 3 (2.87 Å)] and 34.29° [2 0 4 (2.61 Å)]. Whereas the characteristic peaks [h k l (d_{spacing})] of 450 °C calcined (01-070-1402) potassium borate were observed at the 2θ positions of 17.03° [1 1 2 (5.20 Å)], 21.18° [2 0 0 (4.19 Å)], 21.50° [0 2 1 (4.13 Å)], 22.66° [0 2 2 (3.92 Å)], 22.75° [2 0 2 (3.91 Å)], 24.50° [0 2 3 (3.63 Å)] and 26.86° [0 2 4 (3.31 Å)].

The SEM morphologies of the calcined potassium borates are given in Fig. 10, from which it can be seen that round overlapped particles and some rectangular particles were obtained from both the calcination temperatures of 450 and 550 °C, with the increase in the temperature leading to a more uniformly distributed and smooth particles. At 450 °C, the round particles were seen between 394.20 and 1.07 μm, and rectangular particles length were seen at approximately 1.17 μm. At 550 °C, the particle sizes of round articles were found between 684.31 and 1.13 μm, and rectangular particles length were seen at approximately 1.98 μm. So the increase in the calcination temperature leads to bigger particle sizes than 450 °C.

Table 4 Crystallographic data of dehydrated potassium borates

Mineral name	Potassium borate	Potassium borate
Reference code	01-070-1402	01-076-1367
Chemical formula	KB ₅ O ₈	KB ₅ O ₈
Molecular weight (g/mol)	221.20	221.20
Crystal system	Orthorhombic	Orthorhombic
Space group	Pbca (No. 61)	Pbca (No. 61)
<i>a</i> (Å)	8.3830	7.4200
<i>b</i> (Å)	8.4180	11.6900
<i>c</i> (Å)	21.5400	14.7200
α (°)	90.00	90.00
β (°)	90.00	90.00
γ (°)	90.00	90.00
<i>z</i>	8.00	8.00
Density (calculated, g/cm ³)	1.93	2.30

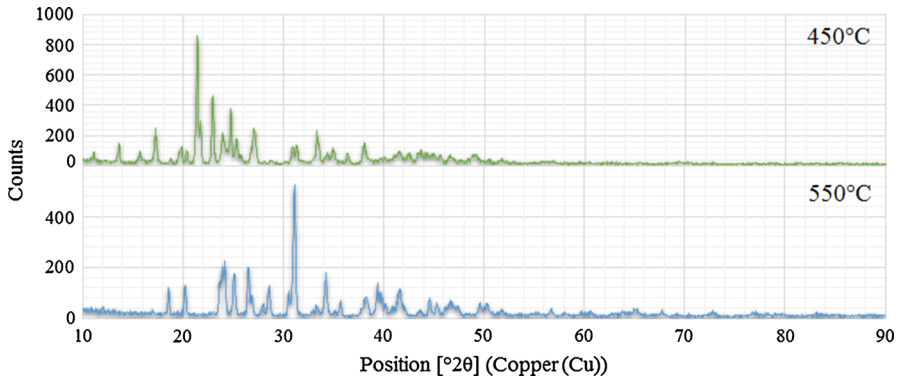


Fig. 9 XRD pattern of calcined potassium borates

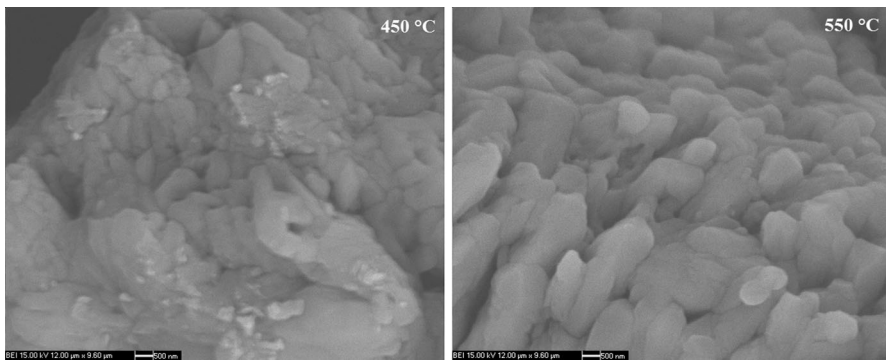


Fig. 10 SEM morphologies of calcined potassium borates

Kinetic results

Coats–Redfern, Doyle, KAS and OFW kinetic methods were applied for the calculation of kinetic parameters such as reaction order (n), activation energy (E_a) and exponential factor (k_0). Calculated parameters for these kinetic methods are given in Table 5.

In the Coats–Redfern method, the n value was determined as 1, the average E_a was 110.12 kJ/mol and k_0 values were in the range of 3.79×10^{12} – 7.06×10^{13} for the first step of dehydration. At the second step of dehydration, n value was determined as 2, average E_a was 202.43 kJ/mol and k_0 values were in the range of 1.76×10^{20} – 1.17×10^{24} .

In the Doyle method, k_0 values were in the range of 9.59×10^{-7} – 1.42×10^{-7} for the first step of dehydration. At the second step of dehydration, k_0 values were in the range of 1.42×10^{-7} – 9.59×10^{-7} . On the other hand, E_a values were determined as 107.77 and 304.18 kJ/mol for the first and second steps of dehydration, respectively.

Table 5 Calculated parameters for kinetic methods

Steps	β (°C/ min)	Coast-Redfern method			Doyle method			α			KAS method			OFW method		
		R^2	k_0	E_a (kJ/mol)	R^2	k_0	E_a (kJ/mol)	R^2	E_a (kJ/mol)	R^2	E_a (kJ/mol)	R^2	E_a (kJ/mol)	R^2	E_a (kJ/mol)	
1st	5	0.9913	7.06×10^{13}	117.11	0.9991	1.42×10^{-7}	107.77	0.1	0.9954	181.97	0.9957	179.47				
								0.2	0.9965	158.17	0.9968	156.98				
		0.9923	3.79×10^{12}	105.75		6.22×10^{-7}		0.3	0.9970	153.98	0.9972	155.46				
20	15						0.4	0.9947	152.42	0.9952	151.68					
							0.5	0.9952	150.35	0.9956	149.77					
		0.9904	6.89×10^{12}	107.51		9.59×10^{-7}		0.6	0.9981	150.48	0.9983	149.96				
2nd	5	Average activation energy		110.12				0.7	0.9988	152.45	0.9989	151.89				
		0.9917	1.17×10^{24}	215.66	0.9947	1.76×10^{-16}	304.18	0.8	0.9999	158.25	0.9999	157.48				
								0.9	0.9932	171.27	0.9938	169.94				
15	20						Average activation energy		158.82	Average activation energy	158.07					
		0.9927	1.21×10^{23}	208.23				0.1	0.9977	171.13	0.9979	191.31				
								0.2	0.9999	154.93	0.9999	154.62				
20	15						0.3	0.9997	145.40	0.9998	145.61					
							0.4	0.9991	144.87	0.9992	145.16					
		0.9893	1.76×10^{20}	183.42		8.17×10^{-16}		0.5	0.9978	152.27	0.9981	152.24				
Average activation energy	202.43						0.6	0.9938	159.81	0.9944	159.47					
							0.7	0.9873	169.72	0.9885	168.96					
							0.8	0.9856	169.45	0.9869	168.78					
							0.9	0.9745	122.95	0.9776	124.70					
							Average activation energy	154.50	Average activation energy	156.76						

Table 6 Published data of kinetic studies related to boron minerals

Borates	Kinetic models	Reaction steps	Reaction degree	k_0 (s^{-1})	E_a (kJ/mol)	References
Ulexite	Suzuki	1	1	9821.8–524.9	47.34–60.01	[17]
$NaCaB_5O_6(OH)_6 \cdot 5H_2O$	C–R					
Boric acid	Suzuki	1	1	6.75×10^6	4.45	[19]
H_3BO_3	C–R	1	1	636.67	79.85	
		2		6.74×10^{-7}	4.79	
Sodium metaborate tetrahydrate	C–R	1	1	0.43×10^4	50.86	[20]
$NaB(OH)_4 \cdot 2H_2O$		2		14.5	18.51	
		3		8.67	15.72	
		4		5.67	4.37	
		5		142.67	37.42	
McAllisterite	Ozawa	1	1	–	100.40	[21]
$Mg_2(B_6O_7(OH)_6)_2 \cdot 9H_2O$	KAS	1	1	3.33×10^{-6} –48.56	98.31	
Admontite	Ozawa	1	1	–	107.72	[22]
$MgB_6O_7(OH)_6 \cdot 3H_2O$		2		–	165.42	
	Kissinger	1	1	5.98×10^{11}	88.79	
		2		1.98×10^{13}	129.78	
	Doyle	1	1	4.01×10^{14}	90.48	
		2		1.44×10^{16}	131.24	
Inderite	Ozawa	1	1	–	87.00	[23]
$2MgO \cdot 3B_2O_3 \cdot 15H_2O$	Kissinger	1	0.99	3.45×10^8	83.00	
	Doyle	1	1	2.90×10^{11}	85.00	
	C–R	1	1.18	3.05×10^{12}	106.00	

Table 6 continued

Borates	Kinetic models	Reaction steps	Reaction degree	k_0 (s^{-1})	E_a (kJ/mol)	References
Zinc borate hydrate	C-R	1	1	1.42×10^{17} – 4.09×10^{18}	225.40	[24]
$Zn_3B_6O_{12} \cdot 3.5H_2O$		2	1	7.43×10^{36} – 8.61×10^{53}	570.63	
	H-M	1	1	2.06×10^{19} – 3.68×10^{20}	254.33	
		2	1	3.17×10^{37} – 2.24×10^{55}	518.22	
Howlite	FOTD	1	1	50.8×10^5	65.00	[26]
$Ca_2B_5SiH_3O_{14}$						
Tunellite	FOTD	1	1	32.5×10^5	50.40	[26]
$SrB_6H_8O_{14}$						

C-R Coats-Redfern, H-M Horowitz-Metzger, KAS Kissinger-Akahira-Sunose, FOTD first order thermal decomposition

In the KAS method, E_a values were calculated as 158.82 and 154.50 kJ/mol for the first and second steps of dehydration, respectively. Similar with the KAS method, in the OFW method calculated E_a values were in the range of 158.07 and 156.76 kJ/mol for the first and second steps of dehydration, respectively.

Kinetic parameters of different borate compounds which are found in the literature are given in Table 6, according to which, hydrated borate minerals generally lose their crystal water in one or two steps except for sodium metaborate hydrate. In general, total activation energies are in the range of 80–120 kJ/mol. The zinc borate hydrate and admontite minerals have higher activation energies than the other types of borate hydrates. Their total activation energies for the dehydration process are approximately 780 and 250 kJ/mol, respectively. Compared to the other borate hydrates, santite mineral's total activation energy is 310 kJ/mol. This high activation energy leads to better heat resistance than the other types of hydrated borates except for zinc borate hydrate and admontite.

Conclusions

In this paper, a potassium borate mineral of santite ($\text{KB}_5\text{O}_8 \cdot 4\text{H}_2\text{O}$) was synthesized from different raw materials at various reaction temperatures (60–90 °C) and reaction times (15–120 min). According to the XRD results, at lower temperatures the crystallinity of the produced $\text{KB}_5\text{O}_8 \cdot 4\text{H}_2\text{O}$ is higher when the reaction yield increases allied with increasing reaction temperature. For the reactions that were taking place with H_3BO_3 and B_2O_3 , the reaction yields reached 95.11 and 89.20 %, respectively. FT-IR and Raman spectra of the products were in conformity with typical peaks of potassium borate in both the infrared and visible regions. On the basis of SEM observations of the specimen, the particle size of synthesized compounds for different reaction sets were found between 666.7 nm and 5.98 μm . Following the synthesis step, dehydration kinetics of the santite mineral were studied and thermogravimetric analyses showed that dehydration of santite occurred in two steps. Coats–Redfern and Doyle non-isothermal kinetic methods were used for the determination of activation energies (E_a) and found to be 110.12 and 202.43 kJ/mol in the Coats–Redfern method for steps 1 and 2. On the other hand, in the method of Doyle, E_a was found as 107.77 and 304.18 kJ/mol for steps 1 and 2. The differences between the E_a can be explained by the variation of the data obtained from different kinetic methods which are compatible with the other study given in the literature [34].

References

1. A.S. Kipcak, E. Moroydor Derun, J. Piskin, J. Chem. **2013**, 329238 (2013)
2. E.M. Derun, A.S. Kipcak, J. Radioanal. Nucl. Chem. **292**, 871 (2012)
3. L.D. Pye, V.D. Frechette, N.J. Kreidl, *Borate Glasses: Structure, Properties, Applications*, 1st edn. (Plenum, New York, 1978)
4. G. Yang, Z. Li, Y. Zhang, Chem. Eng. Process. **44**, 1216 (2005)

5. K. Thamizharasan, S.X. Jesu Raja, F.P. Xavier, P. Sagayaraj, *J. Cryst. Growth* **218**, 323 (2000)
6. S. Merlino, F. Sartori, *Contr. Mineral. Petrol.* **27**, 159 (1970)
7. W.A. Gale, Method of preparing potassium pentaborate. Patented Oct. 5, 1937 (No. 45, 57)
8. W.M. MacDonald, A.-C. Anderson, J. Schoreder, *Phys. Rev. B* **32**, 1208 (1985)
9. Y.S.M. Alajerami, S. Hashim, W.M.S. Wan Hassan, A.T. Ramli, *J. Mol. Struct.* **1026**, 159 (2012)
10. P.R. Binu, C.M. Joseph, C.S. Menon, K. Shreekrishnakumar, *Mater. Lett.* **52**, 323 (2002)
11. S. Hashim, Y.S.M. Alajerami, A.T. Ramli, S.K. Ghoshal, M.A. Saleh, A.B. AbdulKadir, M.I. Saripan, K. Alzimami, D.A. Bradley, M.H.A. Mhareb, *Appl. Radiat. Isotopes* **91**, 126 (2014)
12. O. Sahin, E.S. Cennetkusu, H. Dolas, M. Ozdemir, *Thermochim. Acta* **440**, 7 (2005)
13. E.L. Belokoneva, S.Y. Stefanovich, O.V. Dimitrova, *J. Solid State Chem.* **195**, 79 (2012)
14. G. Wang, Y.G. Sun, S. Zheng, G. Yang, *Z. Anorg. Allg. Chem.* **632**, 1586 (2006)
15. S.A. Rajasekar, K. Thamizharasan, A. Joseph Arul Pragasam, J. Packiam Julius, P. Sagayaraj, *J. Cryst. Growth* **247**, 199 (2003)
16. H. Gurbuz, G. Badem, A.N. Bulutcu, *J. Cryst. Growth* **283**, 222 (2005)
17. M. Tunc, H. Ersahan, S. Yapici, S. Colak, *J. Therm. Anal.* **48**, 403 (1997)
18. A.K. Galwey, *Thermochim. Acta* **355**, 181 (2000)
19. F. Sevim, F. Demir, M. Bilen, H. Okur, *Korean J. Chem. Eng.* **23**, 736 (2006)
20. A. Kantürk, M. Sari, S. Piskin, *Korean J. Chem. Eng.* **6**, 1331 (2008)
21. E.M. Derun, F.T. Senberber, *Sci. World J.* **2014**, 985185 (2014)
22. E.M. Derun, A.S. Kipcak, F.T. Senberber, M.S. Yilmaz, *Res. Chem. Intermed.* **41**, 853 (2015)
23. A.K. Figen, M.S. Yilmaz, S. Piskin, *Mater. Charact.* **6(61)**, 640–647 (2010)
24. A.S. Kipcak, F.T. Senberber, E.M. Derun, N. Tugrul, S. Piskin, *Res. Chem. Intermed.* **41**, 9129 (2015)
25. M. Touboul, E. Betourne, *Solid State Ionics* **84**, 189–197 (1996)
26. Y. Erdogan, A. Zeybek, A. Sahin, A. Demirbas, *Thermochim. Acta* **326**, 99 (1999)
27. M.S. Yilmaz, S. Piskin, *J. Chem. Soc. Pak.* **34(3)**, 526 (2012)
28. J. Yongzhong, G. Shiyang, X. Shuping, L. Lun, *Spectrochim. Acta A* **56**, 1291 (2000)
29. L. Jun, X. Shuping, G. Shiyang, *Spectrochim. Acta* **51A**, 519 (1995)
30. A.S. Kipcak, D.Y. Baysoy, E.M. Derun, S. Piskin, *Adv. Mater. Sci. Eng.* **2013**, 747383 (2013)
31. A.S. Kipcak, E.M. Derun, S. Piskin, *Turk. J. Chem.* **38**, 792 (2014)
32. A.S. Kipcak, M. Yildirim, S.A. Yuksel, E.M. Derun, S. Piskin, *Adv. Mater. Sci. Eng.* **2014**, 819745 (2014)
33. H.S. Fogler, *Element of Chemical Reaction Engineering*, 3rd edn. (Prentice-Hall, New Jersey, 1999)
34. M.S. Yilmaz, A.K. Figen, S. Piskin, *Res. Chem. Intermed.* **41**, 1893 (2015)